ISBN: 978-3-95450-204-2 ISSN: 2673-5350 doi:10.18429/JACoW-IBIC2019-MOBO01

OVERVIEW OF THE BEAM INSTRUMENTATION AND COMMISSIONING RESULTS FROM THE BNL LOW ENERGY RHIC ELECTRON COOLING FACILITY*

T. Miller†, Z. Altinbas, D. Bruno, J. C. Brutus, M. Costanzo, C. Degen, L. DeSanto, K. A. Drees, A. V. Fedotov, W. Fischer, J. M. Fite, D. Gassner, X. Gu, J. Hock, R. Hulsart, P. Inacker, J. Jamilkowski, D. Kayran, J. Kewisch, C. Liu, K. Mernick, R. Michnoff, M. Minty, S. K. Nayak, L. Nguyen, P. Oddo, R. H. Olsen, M. Paniccia, W. Pekrul, I. Pinayev, V. Ptitsyn, V. Schoefer, S. Seletskiy, H. Song, A. Sukhanov, P. Thieberger, J. Tuozzolo, D. Weiss, BNL, Upton, NY, USA

Abstract

The Low Energy RHIC Electron Cooling (LEReC) facility [1] at BNL demonstrated, for the first time, cooling of ion beams using a bunched electron beam. LEReC is planned to be operational to improve the luminosity of the Beam Energy Scan II physics program at RHIC in the following two years. In order to establish cooling of the RHIC Au ion beam using a 20 mA, 1.6 MeV bunched electron beam; absolute energy, angular and energy spread, trajectory and beam size were precisely matched. A suite of instrumentation was commissioned [2] that includes a variety of current transformers, capacitive pick-up for gun high voltage ripple monitor, BPMs, transverse and longitudinal profile monitors, multi-slit and single-slit scanning emittance stations, time-of-flight and magnetic field related energy measurements, beam halo & loss monitors and recombination monitors. The commissioning results and performance of these systems are described, including the latest design efforts of high-power electron beam transverse profile monitoring using a fast wire scanner, residual gas beam induced fluorescence monitor, and Boron Nitride Nano-Tube (BNNT) screen monitor.

INTRODUCTION

Electron cooling of ion beams has been demonstrated long before now but with DC beams. As higher energy electron beams are needed to cool higher energy ion beams, RF acceleration becomes a necessary method. LEReC is the first electron cooler to employ RF acceleration of electron bunches [3, 4], paving the way toward the development of future higher energy electron coolers. The LEReC accelerator is based on a 400kV DC gun with laser-driven [5, 6] photocathode [7], and an SRF booster with a set of three normal conducting RF cavities [8] with which to provide a control of "RF gymnastics" to effectively tune the beam in the longitudinal phase space [9]. The machine layout is shown in Fig. 1. The LEReC beam contains a complex bunch structure defined by the 704 MHz fiber laser producing bunch trains of 40-ps bunches at ~9 MHz to effectively overlap the ion bunches in RHIC, as described in detail in [4].

LEReC was successfully commissioned in 2018 [10] and demonstrated cooling during the 2019 RHIC run with Au ions [4]. Table 1 summarizes the design parameters of the electron beam in the cooling section (CS). Although the designed charge per bunch was obtained, it was found that a lower charge of around 75 pC was most optimal for cooling so far.

Table 1: Electron Beam Parameters in the CS

Electron beam energy, MeV	1.6-2.6
Charge per single bunch, pC	130-200
Number of bunches in macrobunch	30-24
Total charge in macrobunch, nC	3-5
Average current, mA	30-55
RMS normalized emittance, μm	< 2.5
Angular spread, mrad	< 0.15
RMS energy spread	$<5 \times 10^{-4}$
RMS bunch length, cm	3
Length of cooling sections, m	20

BEAM INSTRUMENTATION SYSTEMS

All instruments and associated systems, depicted in Fig. 1, have been described previously in detail in [2]. Descriptions of updates to each instrumentation system are elaborated on in the sections that follow along with the latest commissioning results.

Gun Instrumentation

Laser Exit Monitoring & Cathode Imaging

A laser exit table sits at the laser exit port to receive the drive laser reflected off of the mirror polished surface of the cathode substrate to minimize beam halo & tails otherwise generated by scattered light reaching the cathode. A power meter measures the exit-laser power to predict a loss of light inside the cathode laser chamber. A camera monitors the laser spot on the power meter to allow an operator to check for clipping of the laser spot.

The surface of the cathode substrate, a polished molybdenum puck with an activated cathode spot, held in the DC gun, is imaged, as shown in Fig. 2a. This imaging is used for alignment and automated tracking of the laser spot during automated quantum efficiency (QE) scans. The cathode is illuminated on-axis by an LED spotlight with adjustable spot size to minimize glare from surrounding reflective surfaces. A 2 MP GigE camera, AVT model Manta G201B, is fitted with a Navitar 6x ZoomXtender [11] lens assembly (working distance of 0.3 – 16 m) to image the 25-mm cathode substrate at a distance of 1 m.

ISBN: 978-3-95450-204-2 ISSN: 2673-5350 doi:10.18429/JACoW-IBIC2019-MOB001

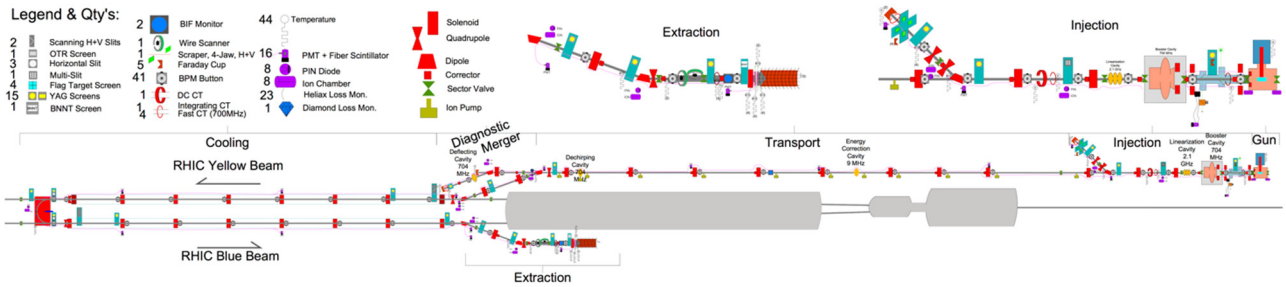

Figure 1: Layout of 100 m long LEReC electron accelerator showing the five sections. An enlarged view of the injection & extraction sections is inset in the view.

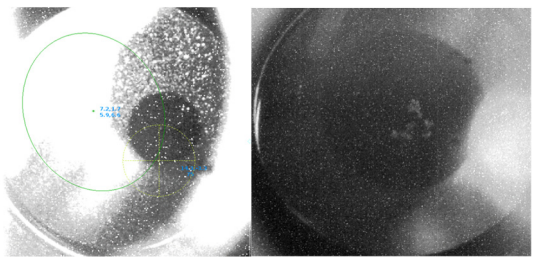

Figure 2: a) Left is the cathode, (2019 run), imaged showing the off-centered 6 mm activated cathode spot. b) Right is a cathode with large centered activated spot from the 2018 run after several ion back bombardments of the cathode during gun trips.

Anode Bias & Ion Clearing

The anode of the gun is biased above ground. The bias power supply was upgraded from 1kV to 3kV to improve the suppression of ion back-bombardment of the cathode. Figure 2b shows the cathode while installed in the gun after it has suffered several of these events. This happened during gun trips. It was found that without this anode bias, we could not produce currents in the milliamp range without tripping the gun. A Keithley 6514 electrometer is connected in series with the power supply's isolated ground return to monitor the anode current. Thus far, no significant anode current has been measured. It is most likely transient in nature only and has not been measured.

Similarly, one set of two opposing 15mm buttons, as used for the BPMs, are installed in the gun-to-booster section with a 500V bias voltage across them to provide an ion clearing electric field across the beam path. The bias is provided by a Keithley 6487 Voltage Sourcing picoammeter. The gun could not operate in the milliamp current range without this bias. Similarly, no dc current has been measured as the events are likely transient in nature. A bias tee has been considered to connect in series in order to study the possible transient nature of the ion clearing.

Gun HV Ripple Monitor

The specification for minimum ripple on the gun high voltage is < 500 V_{RMS}. In order to monitor this, a capacitively coupled pick-up electrode was installed inside the SF_6-filled tank holding the gun HV power supply's active multiplier stack to sample only the variations in the high voltage. A differential amplifier, Tegam model 4040B [12] (DC-100 MHz, 9 nV/Hz-2 input noise) is AC-coupled with a gain of 100 and compares the pick-up signal to the noise of a parallel coaxial cable terminated with a capacitance equivalent to that of the pick-up electrode. An integrator circuit is used to reproduce the ripple waveform. A calibration factor is determined from the measured response to a specific gap in CW beam of a given current, compared to the expected voltage change on the measured capacitance of the pick-up. Significant ripple was found at 166 kHz (twice the power supply switching frequency) as well as at 360 Hz (from the 3-phase rectifier). Initial ripple of > 6 kV_{P-P} was measured before relocating the regulator chassis outside of the accelerator tunnel. Subsequent ripple values were measured at 1 kV_{P-P} and 160 V_{P-P} at 360 Hz and 166 kHz respectively; which are 30% below the maximum 500 V_{RMS} ripple requirement to ensure proper energy spread of the beam to enable cooling.

YAG Screen Profile Monitors

Two YAG screen profile monitors (PM) were added since last reported in [2], now totalling 15 throughout the machine. The illumination of many of the PMs was upgraded to a switchable 450 nm (blue) and white light by installing 60 mm diameter RGB LED rings at the viewport. This allows uniform illumination of the YAG with 450 nm light (YAG:Ce peak absorption) to check the health of the crystal and to provide some patterning on which to help focus the optics. All 15 PM's now employ Prosilica GT1600 cameras with a 1/1.8-type 2MP sensor and a gain of 0 – 26 dB. Its external trigger is synchronized to the electron beam and its exposure times range from 10 µs to 68.7 sec. It is paired with a 50-mm lens, Edmund Optics model 89-938, having a stepper motor driven iris with apertures of f/2.1 to f/95 in 42 increments. This has been largely sufficient except during some quadrupole scans for emittance measurements where beam was highly concentrated. Fixed neutral density (ND) filters have been installed in select PM's for this reason.

Performance with these cameras in the RHIC ring has been very good. Out of 21 GT1600 cameras in LEReC and CeC, a nearby experiment, there were only 5 failures in two runs. There were 3 failures of the iris control, one imaging failure, and one complete camera failure.

High Power Profile Monitor R&D

It was found during the 2018 LEReC run that after developing beam optics in pulsed mode, where YAG PM's can be used, transitioning to continuous "wave" (or CW) mode brought about significantly different beam conditions; making it impossible to tune beam conditions in

ISBN: 978-3-95450-204-2 ISSN: 2673-5350 doi:10.18429/JACoW-IBIC2019-MOBO01

pulsed mode for cooling in CW mode. This imposed the need for a high-power profile monitor that could be used during cooling. The development and implementation of the following three systems began in Sept 2018.

Fast Wire Scanner

The urgent need for a fast wire scanner (FWS) was met with a generous offer from CERN to use one of their early-model rotary beam wire scanners (BWS) used in the SPS at CERN. We received two systems complete with both horizontal and vertical scanners installed in a vacuum tank along with VME crates and controller cards [13] for each. Although extensive impedance modelling and corrections had been done at CERN for the in-vacuum elements [14], modelling with Particle Studio was done at BNL considering the different beam parameters of LEReC. Ferrite absorbers were used to line much of the inside of the tank, as shown in Fig. 3, not only to mitigate perturbation of the low energy LEReC beam, but to prevent induced currents

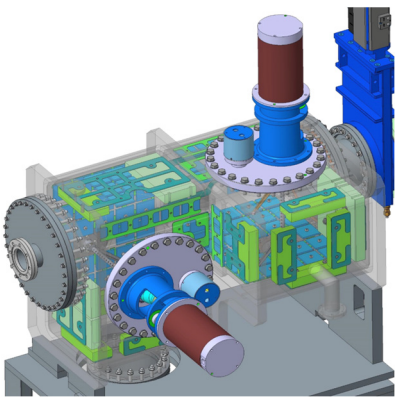

Figure 3: Fast wire scanner vacuum tank with Vert. & Horiz. motors, from CERN SPS, in semi-transparent view showing BNL designed ferrite absorbers inside.

from melting the 50-µm wire we chose to use. The fork tips were redesigned for lower capacitance and an in-vacuum series 1 MΩ resistor was added to reduce the RF currents in the wire induced by the beam that capacitively couple to ground. The signal representing the beam profile will be taken from both the secondary emission signal as the wire interacts with the beam as well as from a scintillator and photomultiplier tube in air.

Both systems were set up and tested, one for operation in the LEReC accelerator and the other as a laboratory test bench. Installation was planned for operation in 2019 but was delayed.

Beam Induced Fluorescence (BIF)

A blackened vacuum chamber and intensified imaging system were built to observe the profile of the electron beam as it causes fluorescence in the residual gas of the vacuum. As the operational pressure is typically in the 10^{-10} torr range, a tungsten filament in the vacuum chamber was added to temporarily increase the pressure to the 10^{-6} torr range. The long transport line with its distributed ion pumps created a local pressure bump, maintaining pressures in the 10^{-10} torr range at the upstream and downstream ends of the 36m-long transport line, as shown in Fig. 4 with measured values at each ion pump along the beamline. Although this worked well, the repeatability diminished as the filament outgassed too much. We will consider adding a gas injection system.

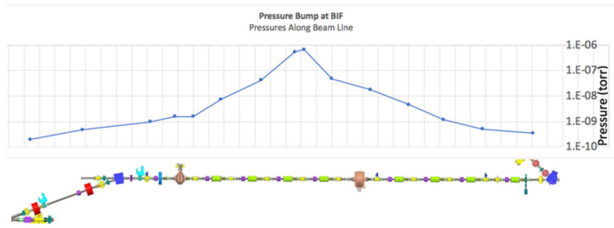

Figure 4: Local pressure bump produced in the transport & merger lines by a filament in the BIF vacuum chamber.

In order to detect the faint emission from the beam induced fluorescence (BIF) in such a low pressure, an industrial camera, Allied Vision Tech. model GT1930, with exceptionally low noise (dark current of 3.3e$^-$) was chosen to be coupled with a fast (/f=0.95), Navitar model DO5095, 50mm lens with an image intensifier between them. The intensifier chosen was a based on a 18mm single-stage MCP with a Hi-QE Green photocathode behind a glass input window and a P43 output phosphor on a fiber-optic plate, having a gain of 9,000 – 11,000. This was procured as model PP3050G from Photonis [15] and housed within their C-mount lens coupling unit called the "Cricket." Lens spacers were added to reduce the working distance of the lens so that it could be placed only two inches from the viewport to increase the solid angle of light collection at the risk of radiation damage.

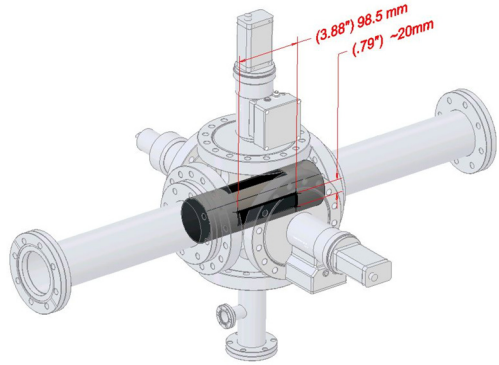

Figure 5: BIF vacuum chamber in semitransparency showing the Magic Black coated drift tube and viewing slots for vertical (side) and horizontal (top) profiles.

Since the inside of the stainless-steel vacuum chamber is very reflective, a background with a light absorbing coating with low outgassing [16] is necessary. This black coating must be bakeable to 200°C, have outgassing below 10^{-10} torr l/s cm^2, and be electrically conductive enough to bleed off collected charge. After reviewing Diamond-like carbon, Vanta Black™ [17], Singularity™[18], and "Laser Black" [19], it was Magic Black™ [20] that met all requirements with an advertised outgassing of $1\text{x}10^{-13}$ torr l/s cm^2 and a surface resistivity ≤ 2 kΩ/□. Magic Black is a plasma assisted coating process that is difficult to apply to complex shapes. We chose to coat a split cylinder with

ISBN: 978-3-95450-204-2 ISSN: 2673-5350 doi:10.18429/JACoW-IBIC2019-MOB001

slots through which to view the beam, as shown in Fig. 5. These inner cylinder pieces were shipped to Israel for coating and back for assembly.

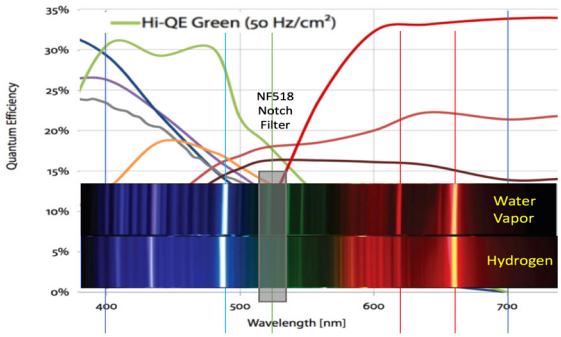

Figure 6: Spectral sensitivity of the "Hi-QE Green" cathode in the intensifier and the principle emission of the residual gas and the notch filter cutting out the green cathode drive laser light.

The optics were housed in light-tight enclosures with interlock switches to cut power to the intensifiers in case of opening to ambient light. The first test unit was installed in the transport line, downstream from the gun. To minimize any stray laser light propagating down the beam pipe from entering the camera, a custom laser line notch filter was purchased for OD6 transmission @ 518 nm (22 nm wide). This was installed on a mirror flipper to remotely control the insertion of the filter in front of the camera lens to test the effect. The expected residual gases were primarily hydrogen and water vapor with emission lines shown in Fig. 6. The "Hi-QE Green" cathode was chosen for the intensifier to have a sensitivity above the green laser light and to collect the strong blue emission line.

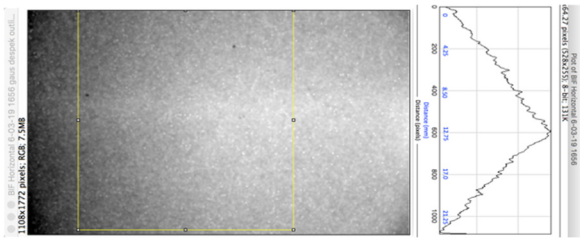

Figure 7: Beam image, gaussian filter, de-speckled, profile averaged horizontally over yellow region of interest.

Long exposures of 1 – 5 seconds were used to acquire images with the maximum camera gain of 40dB. Most collected images showed a response proportional beam current and steering of the beam. This was most likely the intensifier's response to Bremsstrahlung radiation. Only one partially successful image was acquired, shown with its profile in Fig. 7, but suffers greatly from interference. We will consider adding a lead chicane to the optics path to shield the intensifier.

Boron Nitride NanoTube Screen

A brand-new material has possibly great potential for imaging high power particle beams. Boron Nitride NanoTubes (BNNT) are being produced [21] and formed into uniform papers called "Buckypaper" as thin as 50 µm. This is a low-Z, low areal density (1.0 mg/cm^2) material with an expected working temperature in vacuum of over 900 °C. Preliminary tests with were made by Kevin Jordan at JLAB with a 10 GeV 11nA electron beam that showed clear emission near 480 nm, as shown in Fig 8a. Recent tests of a 60mm diameter BNNT screen with LEReC 1.6 MeV beam showed that detectable emission started at 20 nC with 10 MB's of pulsed beam (over 1.142 µs). Fig. 9 compares the emission of the BNNT screen to that of a YAG screen. At 25 nC, the BNNT emission was a mere 0.41% that of the YAG screen (based on comparing the f/2.1 aperture setting for the BNNT to the f/32 setting for the YAG). This test also showed that the scattering of the electrons passing through the BNNT screen was only 20% that of the YAG screen. Thus, the dump has a better chance of collecting all the beam at high power. Calculations predict a scattering angle of 25 – 35 mrad.

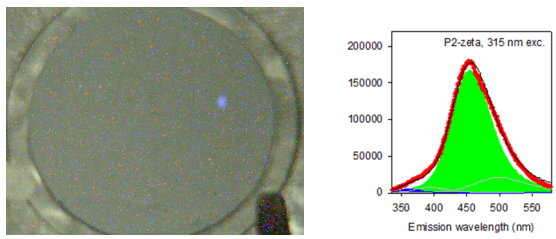

Figure 8: a) Left: Blue spot showing emission of BNNT screen under 10 Gev electron beam at 11 nA. b) Right: expected emission spectrum of the BNNT screen. (Images courtesy of Kevin Jordan, BNNT, LLC.)

The screen will be installed a few centimeters upstream of the defocusing solenoid at the entrance of the dump in order to allow the dump to capture all the scattered beam. Moreover, the beam at this point is large with a 14mm sigma radius (~70 mm max diameter). As the screen will be inserted at a 45° angle to the beam, a BNNT screen size of 120 x 120 mm is required. Driven by a DC motor linear actuator, the screen mounted in a "U-shaped" frame made of Invar, will have one side unsupported so that it can be inserted & extracted during CW beam operation with no metal parts interacting with the beam.

As the screen is intended to intercept the full power electron beam of 1.6 MeV at 38 mA, given its thickness of 50 µm and areal density of 1.0 mg/cm^2, the *dE/dx* heating of the screen mounted at 45° is calculated to be near 100 W with a central temperature of 780 °C. As the thermal conductivity of 0.65 W/mK is not high enough to affect the temperature, this power will be radiated by black-body radiation only and will be "red hot". For temperatures near 1000 °K, the thermal emission in red is four orders of magnitude higher than in blue. This will cause the screen to glow red-orange much brighter than any blue emission due to *dE/dx* ionization or optical transition radiation (OTR). Therefore, the camera will be equipped with a 500 nm OD4 short-pass filter to cut out the thermal emission component below 500 nm and pass the non-thermal emission, centered near 450 nm, as shown in Fig. 8b. To further discriminate the non-thermal emission, a thermal background image will be taken for subtraction from the image of interest. This will be acquired by triggering an exposure the moment the beam is turned off to capture the thermal emission

ISBN: 978-3-95450-204-2 ISSN: 2673-5350 doi:10.18429/JACoW-IBIC2019-MOBO01

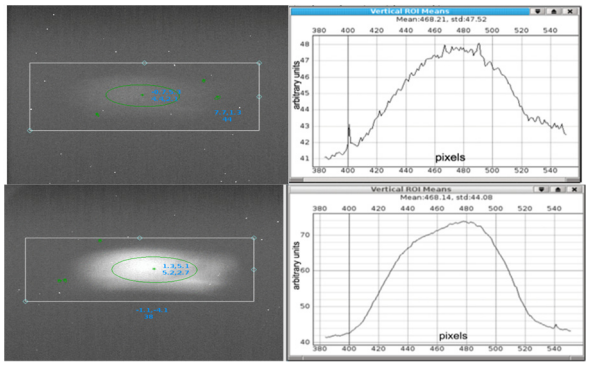

Figure 9: Test with electron beam of 1.6 MeV at 25 nC pulse. Vertical profile calibration is 25.4 pixels/mm. a) Top: BNNT image at f/2.1and vertical profile, b) Bottom: YAG image at f/32 and vertical profile.

without the non-thermal emission. For greatest optical sensitivity, a Prosilica GT1930 camera with Navitar DO5095 f/0.95 50mm lens will sit only 1 inch from the viewport (again at the risk of radiation damage). The camera will be mounted at a Scheimpflug angle to tilt the focus plane to match the 45° angle of the screen. A filter wheel will also be installed to aid the imaging of the intense thermal emission. A ZnSe viewport will be mounted to the opposite port of the vacuum chamber in the event we need to characterize the thermal distribution over the screen.

The main unknown is to what degree the high temperature of the screen will affect the non-thermal emission.

Charge and Current

Beam charge and current is measured, as described in [2], by four custom narrow-band FCT's, one ICT, one DCCT, all made by Bergoz, [22] and four Faraday Cups (FC) – one insertable and three in the beam dumps. The ICT is used during pulsed mode while the DCCT is used during CW mode and with pulse trains > 100 µs. The FC's are used in all modes along with the FCT's which are used in conjunction with the machine protection system (MPS).

The first FCT in the injection section is used by the MPS to trip if the beam current exceeds the limit of the current specified by the auto-detected machine mode, based on beam destination [23]. The subsequent three FCTs, upstream of each beam dump (Injection, Diagnostic, and Extraction) are used by the MPS to trip on beam loss by differential current measurements along trajectories toward each beam dump.

The ICT in the injection section has proved useful to provide a well calibrated charge measurement with beam trains under 7 µs and a maximum charge up to 40 nC. A new application, described in detail in [24], was developed to integrate and analyze the ICT's waveform on a Keysight DSO-X-3024 Oscilloscope to extend the measurement range to long pulses as well as CW.

The DCCT, although originally intended for differential operation [25] between injection and extraction, is now only installed in the injection section. The NPCT electronics [22] are kept in a temperature-controlled chassis to stabilize its response. During commissioning of CW beam, the DCCT provided the most reliable current measurements and was used with the Faraday Cups for transport efficiency measurements as well as to calibrate the FCTs and the ICT (during use with the oscilloscope application). Additionally, a copy of the DCCT output is provided to the Zynq measurement system for comparison with the Faraday Cups; the difference measurement is used for loss detection and connected to the MPS.

Given the 700 MHz structure of the macro-bunches (MB), the custom designed narrow-band FCT signals are connected to power detectors, as shown in Fig. 10, to measures the power of each burst and provide logarithmically proportional voltages. Current measurements are derived by code written for the Zynq FPGA applying an antilog and long-term integration to the signals. This code also determines machine operating states based on predetermined current levels. Discrete outputs provide indication of the beam current level, as determined by the gun FCT, to the MPS. The differential measurement between the gun FCT and the three downstream dump FCTs provide the MPS [26] with differential current loss detection.

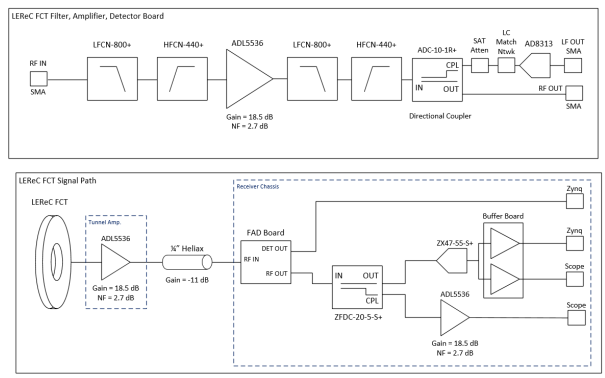

Figure 10: Block diagram of the FCT detector scheme and signal path.

FCT Commissioning Results

The FCTs were capable of measuring pulsed and CW beams over the full charge range of 0.5 – 200 pC/bunch; however, the calibration was inconsistent with non-linearities. To correct for the non-linearity, the Zynq firmware will be updated to allow for non-linear scaling. As an alternative approach, the outputs of the FCTs were directly sampled by a BNL designed digitizer module, V301 [27] used in the BPM system, in parallel with the logarithmic power detectors. With direct digitization, the charge could be measured for each pulse or averaged over multiple pulses. The results showed improved accuracy and linearity, however over a smaller charge range. Further development is planned.

The gun FCT also suffered from noise emanating from the 704-MHz Booster cavity as well as broadband EMI resulting in unnecessary trips of the MPS. In order to reduce the broadband noise and EMI, the analog front-end power supply lines were updated with common mode chokes and the chassis was changed to a solid metal enclosure with all holes covered by copper tape. This effectively eliminated the EMI from the measurement. The remaining Booster cavity noise was in band and could not be filtered out. This

ISBN: 978-3-95450-204-2 ISSN: 2673-5350 doi:10.18429/JACoW-IBIC2019-MOBO01

was corrected by adjusting the noise floor rejection threshold. As a trade-off, the range of minimum measurable charge for pulsed mode was decreased but not significantly. Currents down to 0.2 mA (0.73 pC/pulse) in CW mode can be measured above the Booster cavity noise.

Beam Position Monitor

The strictest requirement for position monitoring is a 50-µm relative accuracy between the electron and ion beams in the cooling section where the angle between them of < 100 µrad is necessary for effective cooling. The 40 Button-style BPM stations, as previously described in [2, 28], consist of three button sizes and two types of electronics. Libera Brilliance Single Pass units monitor 16 stations while 41 V301 modules [27] monitor the other stations. The 17 cooling section stations are monitored by dual V301 modules, one filtered to respond to the RHIC 9 MHz bunches and one filtered to respond to the LEReC 704 MHz structure.

The originally planned scheme of alternately measuring positions of electron bunches in the RHIC abort gap and a single ion bunch, once per turn, was abandoned due to the limited power collected at the 76 kHz RHIC revolution frequency. Instead, both electronics have filters that are continuously rung by the bunch frequencies of the respective bunch train. Position alarms in both electronics platforms are used with 12-µs response times to trip the MPS.

Another reason for not using the abort gap for 9MHz electron-only measurements was that it was found during commissioning that the ions kick the electrons slightly. During the abort gap this kick is not present, and so the electron trajectory differs from that when the beams are both present. Instead, the method used to match BPM measurements from the 9-MHz V301 cards with that of the 704-MHz cards was to first measure the ion beam trajectory in the drift space and adjust all BPM offsets to fit a straight line (ion beam-based alignment). Then only the electron beam was injected and the same 9-MHz BPMs were used to adjust the electron beam trajectory. At the same time, the 704-MHz BPMs were then adjusted to match the 9-MHz BPMs. Once the ion beam was injected, the 9-MHz BPMs then measured a combination of both beams (limited usefulness), but the 704-MHz BPMs could be used to track the electron beam position only. Drifts in the electron trajectory were monitored in this way.

A fast feedback serial link was implemented from the BPM system to the RF system to continuously adjust the beam energy by RF voltage based on beam position in the energy spectrometer built around the 180° dipole magnet in the cooling, as described in detail in [2, 29].

A new mode of beam operation was implemented to provide one LEReC bunch train, of varying length, at a rate of one pulse train per RHIC turn at 76 kHz. The BPM electronics were tuned to operate in this mode.

During operation in CW mode, unexpected response of some BPMs was observed along with failure of some local amplifier electronics in the tunnel. This was suspected to be caused by direct strikes of beam halo to the BPM buttons. This was mitigated by the installation of PIN diode limiters, Minicircuits model ZFLM- 43-5W+. This has effectively prevented recurrence of such failures.

The biggest concern is currently that under some beam conditions, 9-MHz ion beam position measurements diverge considerably from 704-MHz electron beam position measurements. It has been observed that some changes in electron beam charge, while electron and ion beams are interacting, result in a change in the measured position and manifests differently, gradually along the cooling section. This will be investigated in detail during the next run with varying beam conditions to find the cause.

Radiation and Beam Loss Monitoring

While two Canberra AM-IP100 calibrated radiation monitors (100 µR/h – 100 R/h) are used for automated HV conditioning of the gun; the primary protection from beam loss has been the scintillating fiber beam loss monitor system, as described in detail in [2]. The two 8-ch beam loss electronics cards, developed for the JLAB CEBAF upgrade [30], monitor 16 PMTs connected to the fibers. Although this PMT based BCF-60 1-mm diameter scintillating plastic optical fiber (POF) system has successfully protected LEReC from beam loss > 40 nA in under 12 µs over the past two years, the increased power of testing in CW mode has caused ~17% darkening in some of the fibers. Therefore, an undoped quartz fiber was tested and found to have a response of 85% of that of the POF; which can be compensated for with increased bias voltage. Thus, a 1,500 µm quartz fiber in armoured sheath with SMA terminations, ThorLabs M107L02, will be ordered in 16 lengths of 3 – 13 m to replace the POF covering the entire 100 m of the LEReC beam line.

Libera™ BLM Test

A test of the Libera BLM 4-channel electronics, from Instrumentation Technologies [31], was made in August of 2018 with one of the PMT+scintillating fibers in LEReC. The PLL in the Libera BLM was successfully locked to the RHIC revolution frequency clock @ 78.22 kHz. This allowed the capture of the LEReC macrobunch structure in the beam loss data collected. The control of the mask timing was tested as follows: 1) The LEReC beam was set up for 9 macrobunches (MB) at 1 Hz. 2) The Libera BLM mask was set for a window 9 MB's wide (~117 clock cycles). 3) The mask timing was shifted by 13 clock cycles at a time to effectively shift the window over the lost beam pulse train by one LEReC MB at a time; which showed a linear response in the sum data where the masked window rolled through the time where the beam could be detected.

This showed that the Libera BLM can be used to sample the beam only in the RHIC abort gap so as to be insensitive to the RHIC beam losses and only sensitive to the LEReC beam losses with ~11us gaps in the sampling of the beam loss (effectively sampling ~1us out of every RHIC turn at ~78 kHz). This method may be used in the future to mitigate gun trips during RHIC injection losses.

ISBN: 978-3-95450-204-2 ISSN: 2673-5350 doi:10.18429/JACoW-IBIC2019-MOB001

Emittance & Energy Spread

Emittance and energy spread are measured using insertable slits and profile monitors, as described earlier in [2, 23]. Normalized emittance was successfully measured to be < 1.6 μm in both cooling sections using scanning slits and < 2.5 μm in the injection section with a multislit, as described in detail in [10], beating the 2.5 μm requirement for cooling. The Longitudinal Phase Monitor, based on an RF deflecting cavity in the RF diagnostic beam line, described earlier in [2], was used to measure the energy spread of $2x10^{-4}$ (400 eV) as described in detail in [10], beating the $5x10^{-4}$ requirement for cooling.

Energy Measurement and Matching

Absolute energy of the electron beam is measured in two ways; by the time-of-flight energy measurement system, and by the magnetic energy spectrometer, previously described in [2, 32] with commissioning results given in [33] and [29] respectively. An NMR-20 Gaussmeter [34], previously used to map the field of the spectrometer's dipole magnet [35, 36], is permanently installed to monitor the magnet's field during operation. Logged data shows a low noise of < 20 milligauss and a deviation from fill to fill of < 3 milligauss over an 8-hour period. The measured field is used with the beam position displacement measurement to automatically calculate the beam energy.

In an effort to match electron and ion beam energies, a recombination monitor, described previously in [2] with commissioning results given in [29], is used as an indicator of proper alignment and energy match of the electron and ion beams. In addition to the high-speed counters that have logged event rates of up to 8 kHz, two Agilent 53230A time digitizers were installed to provide bunch-by-bunch recombination values synchronized to each RHIC bunch.

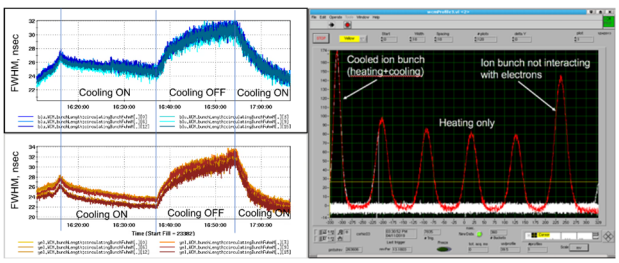

he "Roadmap to cooling" [4] involves a multi-step process of

Figure 11: Cooling reduces bunch length measured by WCM, a) Left: in both RHIC rings with cooling ON, OFF and ON, and b) Right: WCM scope trace during cooling.

The "Roadmap to cooling" [4] involves a multi-step process of matching the electron energy to that of the ions with 10^{-4} accuracy [29]; where the electron energy is set in four steps. First, the RF voltage is set. Second, the energy is measured with the magnetic spectrometer. Third, the RF phase is adjusted in steps of 1 kV of accelerating voltage to minimize recombination rate with electron – ion overlap. Fourth, the RF phase is adjusted in steps of 100 V of accelerating voltage to minimize ion bunch width, measured by the RHIC wall current monitor (WCM) [37] during cooling. Although described in detail in [4], Fig. 11a shows the evolution of the RHIC bunch length as measured by the WCM as cooling is turned on, then off, then on again during a RHIC store. Fig. 11b shows a trace from the WCM scope with one ion bunch being cooled in 76 kHz mode (where beam loading only affords one electron MB at the matched energy for cooling) while other are heated. Note the cooled bunch is improved over the noninteracting one. Progress of cooling was also shown by monitoring the average bunch width using the RHIC H-JET profile monitor [38]. Fig. 12 shows the precision of measured values compared to those predicted during the conception of the instrumentation.

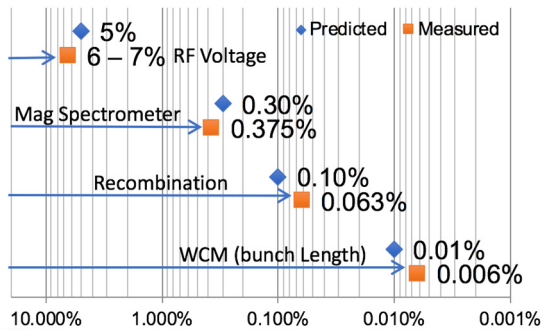

Figure 12: Predicted vs measured energy matching values.

CONCLUSION

LEReC will make its first operational run beginning in December, cooling RHIC ion beams over the next two runs in support of the low end of the beam energy scan program in search of the critical point on the QCD phase diagram. All instrumentation is ready for operations, except for the high-power profile monitors. R&D will continue for the FWS, BIF and BNNT in case this becomes a necessary diagnostic to ensure reliable cooling during operations.

ACKNOWLEDGEMENTS

The authors would like to acknowledge the contributions of R. Jones, F. Roncarlo, J. Emery, and R. Veness for their contributions and support of the SPS wire scanner system, as well as Kevin Jordan and Roy Whitney with BNNT, LLC for their work to customize the BNNT screen, and Cyrille Thomas with the ESS for help with the calculations for the BIF project, as well as Cedric Germain with Caylar for support of the NMR Gaussmeter, and M. Cargnelutti with Instrumentation Technologies for the loan of the Libera BLM electronics. Special thanks also go to members of the Accelerator Components & Instrumentation Group, especially A. Curcio, and D. Lehn, as well as members of the design room, especially K. Hamdi and M. Grau.

REFERENCES

[1] A. V. Fedotov *et al.*, "Accelerator Physics Design Requirements and Challenges of RF Based Electron Cooler LEReC", in *Proc. NAPAC'16*, Chicago, IL, USA, Oct. 2016, pp. 867-869. doi:10.18429/JACoW-NAPAC2016-WEA4CO05

ISBN: 978-3-95450-204-2 ISSN: 2673-5350 doi:10.18429/JACoW-IBIC2019-MOB001

[2] T. A. Miller *et al.*, "LEReC Instrumentation Design & Construction", in *Proc. IBIC'16*, Barcelona, Spain, Sep. 2016, pp. 417-421. doi:10.18429/JACoW-IBIC2016-TUPG35

[3] D. Kayran *et al.*, "Commissioning of the Electron Accelerator LEReC for Bunched Beam Cooling", presented at the NAPAC'19, Lansing, MI, USA, Sep. 2019, paper TUZBA1.

[4] A. V. Fedotov *et al.*, "First Electron Cooling of Hadron Beams Using a Bunched Electron Beam", presented at the NAPAC'19, Lansing, MI, USA, Sep. 2019, paper THZBA5.

[5] P. Inacker *et al.*, "Design of the 2-Stage Laser Transport for the Low Energy RHIC Electron Cooling (LEReC) DC Photogun", presented at the NAPAC'19, Lansing, MI, USA, Sep. 2019, paper MOPLM18.

[6] L. K. Nguyen *et al.*, "Active Pointing Stabilization Techniques Applied to the Low Energy RHIC Electron Cooling Laser Transport at BNL", presented at the NAPAC'19, Lansing, MI, USA, Sep. 2019, paper THYBA6.

[7] E. Wang *et al.*, "Bi-Alkali Antimonide Photocathodes for LEReC DC Gun", in *Proc. IPAC'19*, Melbourne, Australia, May 2019, pp. 2154-2156. doi:10.18429/JACoW-IPAC2019-TUPTS101

[8] S. A. Belomestnykh *et al.*, "SRF and RF Systems for LEReC Linac", in *Proc. IPAC'15*, Richmond, VA, USA, May 2015, pp. 3600-3602. doi:10.18429/JACoW-IPAC2015-WEPWI050

[9] J. Kewisch, A. V. Fedotov, D. Kayran, and S. Seletskiy, "Beam Optics for the RHIC Low Energy Electron Cooler (LEReC)", in *Proc. NAPAC'16*, Chicago, IL, USA, Oct. 2016, pp. 1015-1017. doi:10.18429/JACoW-NAPAC2016-WEPOB56

[10] D. Kayran *et al.,*"First results from commissioing of low energy RHIC electron cooler (LEReC)", in *ProcIPAC2019*, Melbourne, Australia, May 2019, pp. 770-772. doi:10.18429/JACoW-IPAC2019-MOPRB085

[11] 12X Zoom 6000 Lens System, Navitar, Rochester, NY, https://navitar.com/products/imaging-optics/high-magnification-imaging/

[12] Tegam, Geneva, OH, https://www.tegam.com

[13] S. E. Forde, "Wire Scanner Motion Control Card" CERN, Geneva Switzerland, Rep. CERN-THESIS-2007-032, Dec. 20, 2006.

[14] E. Piselli *et al.*, "CERN-SPS Wire Scanner Impedance and Wire Heating Studies", in *Proc. IBIC'14*, Monterey, CA, USA, Sep. 2014, paper MOPF16, pp. 88-92.

[15] Image Intensifiers, Photonis, Roden, Netherlands, https://www.photonis.com/products/hi-qe-photocathodes

[16] E. D. Erikson, D. D. Berger, B. A. Frazier, "A comparison of the Outgassing Characteristiics of Several Solar Absorbing Coatings", *Journal of Cacuum Sciences & Technology,* A 3, 1711 (1985).

[17] Vanta Black coating by Surrey Nanosystems, New Haven, UK, https://www.surreynanosystems.com/vantablack

[18] Singularity black coating by NanoLab, Waltham, MA, USA, https://www.nano-lab.com

[19] Laser Black coating, Epner Technology, Inc., Brooklyn, NY, USA, https://www.epner.com/processes-and-products/laser-black/

[20] Magic Black coating by Acktar Advanced Coatings, Kiryat Gat, Isreal, https://www.acktar.com

[21] "Bucky Paper" from BNNT, LLC, Newport News, VA, USA, https://www.bnnt.com/

[22] Bergoz Instrumentation, Saint Genis Puilly, France, https://www.bergoz.com/en

[23] P. Piot *et al.*, "A Multislit Transverse-Emittance Diagnostic for Space-Charge-Dominated Electron Beams", in *Proc. PAC'97*, Vancouver, Canada, May 1997, paper 5P064, pp. 2204 – 2206.

[24] M. Paniccia, et al., "Python Based Application for Beam Current Transformer Signal Analysis", presented at ICALEPCS'19, New York, NY, USA, October 2019, not yet published.

[25] P. Cameron, "Differential Current Measurement in the BNL Energy Recovery LINAC Test Facility", C-AD, Brookhaven National Lab, Upton, NY, Rep. C-AD/AP/203, August, 2005.

[26] S. Seletskiy *et al.*, "Conceptual Design of LEReC Fast Machine Protection System", in *Proc. IBIC'16*, Barcelona, Spain, Sep. 2016, pp. 665-668. doi:10.18429/JACoW-IBIC2016-WEPG19

[27] R. L. Hulsart, P. Cerniglia, N. M. Day, R. J. Michnoff, and Z. Sorrell, "A Versatile BPM Signal Processing System Based on the Xilinx Zynq SoC", in *Proc. IBIC'16*, Barcelona, Spain, Sep. 2016, pp. 646-649. doi:10.18429/JACoW-IBIC2016-WEPG12

[28] Z. Sorrell, P. Cerniglia, R. L. Hulsart, K. Mernick, and R. J. Michnoff, "Beam Position Monitors for LEReC", in *Proc. IBIC'16*, Barcelona, Spain, Sep. 2016, pp. 47-50. doi:10.18429/JACoW-IBIC2016-MOPG08

[29] S. Seletskiy *et al.*, "Precise Beam Velocity Matching for the Experimental Demonstration of Ion Cooling with a Bunched Electron Beam", presented at the NAPAC'19, Lansing, MI, USA, Sep. 2019, paper TUZBB3.

[30] J. Yan and K. L. Mahoney, "New Beam Loss Monitor for 12 GeV Upgrade", in *Proc. ICALEPCS'09*, Kobe, Japan, Oct. 2009, paper WEP092, pp. 582-584.

[31] Libera BLM system, Instrumentation Technologies, Solkan, Slovenia, https://www.i-tech.si/products/libera-blm/

[32] T. A. Miller *et al.*, "Multifunction Instrument Designs with Low Impedance Structures for Profile, Energy, and Emittance Measurements for LEReC at BNL", in *Proc. IBIC'15*, Melbourne, Australia, Sep. 2015, pp. 307-312. doi:10.18429/JACoW-IBIC2015-TUPB007

[33] I. Pinayev, et al, "Time of Flight Technique for Matching Energies in Electron Cooler", presented at IBIC'19, Malmo, Sweden, Sept. 2019, paper WEPP043, this conference.

[34] CAYLAR, France, http://www.caylar.net/

[35] T. A. Miller *et al.*, "Low Field NMR Probe Commissioning In LEReC Energy Spectrometer", in *Proc. IBIC'17*, Grand Rapids, MI, USA, Aug. 2017, pp. 423-427. doi:10.18429/JACoW-IBIC2017-WEPCF05

[36] H. Song, et al. "Magnetic Field Measurement and Mapping of the LEReC 180 Bending Magnet Using High-Precision Low Field NMR Probe (<140 Gauss)", in *Proc. International Magnetic Measurement Workshop 2019*, Grenoble, France, June, 2019, not yet published.

[37] Barsotti, E.L.; Cameron, Peter R.; Crisp, Jim; Fellenz, Brian; Shea, Thomas J.; Lee, Roger C.; van Zeijts, Johannes, "The RHIC Wall Current Monitor System", in *Proc. PAC'99*, New York, NY, USA, Mar. 1999, paper WEA116, pp. 2146-2148.

[38] T. Tsang *et al.*, "Optical Beam Profile Monitor at the RHIC Polarized Hydrogen Jet", in *Proc. PAC'09*, Vancouver, Canada, May 2009, paper TH5RFP019, pp. 3485-3487.